RSC Advances

ROYAL SOCIETY OF CHEMISTRY

www.rsc.org/advances

Flexible hollow CeO_2/Al_2O_3 fibers: Preparation, characterization and dye adsorption efficiency

Xing-hai Zhou[1], Wei-min Kang[1*], Wei Xu[1], Bo-wen Cheng[1,2*]

1. School of Textiles, Tianjin Polytechnic University, Tianjin 300387, China

2. Key Laboratory of Advanced Textile Composite Materials, Ministry of Education of China, Tianjin 300387, China

Abstract

Flexible hollow CeO_2/Al_2O_3 fibers were successfully prepared, for the first time, by coaxial electro-blowing spinning technique. Diameter of these fibers could be controlled by adjusting spinning parameters. Upon sintering the as-spun fibers at 600 ℃, flexible hollow CeO_2/Al_2O_3 fibers were obtained with continuous morphologies. Their microstructure was characterized by scanning electron microscopy (SEM), X-ray photoelectron spectrum (XPS), X-ray diffraction (XRD) and specific surface area (BET). Dye removal experiment was evaluated from the adsorption efficiency of Methyl Orange (MO) in aqueous solution. That exhibited strong adsorption capacity of MO molecules in dark condition and were easily separated by simple filtration, thus showing promise for application in wastewater treatment and environmental purification.

Key words: X-ray methods, sintering, flexible hollow CeO_2/Al_2O_3 fibers, coaxial electro-blowing.

1. Introduction

With the development of industrialization, environmental pollution is becoming more and more serious. Especially water pollution caused by the textile dyes which is difficult to solve [1]. So it is urgent to find an efficient material with rapid removal capacity of dye under mild conditions. To overcome this problem,

*Corresponding author. E-mail addresses: kweimin@126.com (W. Kang), bowen15@tjpu.edu.cn (B. Cheng).

various micro/nanostructures such as nanoparticles [2], porous microspheres [3], nanotubes [4] have been reported. These materials have superior adsorption capacity for its large specific surface area [5-6].

Cerium (Ce), as a fascinating rare earth element, is one abundant material [7]. Cerium and cerium oxide have attracted much attention due to their high oxygen storage capacity [8-10]. Because of the unique property, they are widely used as catalysts, especially in the removal of organics from wastewaters [11]. CeO_2 fibers with hollow structure have strong adsorption capacity which is propitious to accelerate the adsorption of dyes [12-13]. However, pure ceria textural stability is not high enough to achieve recycling after wastewater treatment [14]. Alumina is widely used as skeleton materials or catalyst support for its excellent mechanical properties and thermal stability [15]. It is also reported that Al_2O_3 fibers had been used as adsorbents for removing dyes [16].

In last decade, a large number of advanced micro/nanofibers have been prepared with well-controlled morphology by various techniques. Notably, among all these 1D nanofibers, hollow fibers have been extensively studied for a strong adsorption capacity and its application in materials [17-19]. Hollow fibers exhibit high specific surface area due to their special hollow structure and small diameter. According to Zhang J et al., micro/nano-scale hollow TiO_2 fibers were successfully prepared through an electro-spinning method [20]. Chang W et al. fabricated hollow TiO_2 nanofibers by the coaxial electrospinning method with enhanced photocatalytic activity [21]. Coaxial electrospinning is currently one conventional technique to produce hollow fibers [22]. However, fibers prepared by this method were obtained in a low production capacity (e.g. 1.0-5.0 mL/h of injection rate) [23], which limited its large-scale application. Recently, a novel solution blowing method with high production rate had been proposed by Cheng B et al [24].

Concerning all the advances of coaxial electrospinning and solution blowing technique, we developed a novel method coxial electro-blowing spinning to prepare flexible hollow CeO_2/Al_2O_3 fibers. Diameter of the as-spun fibers could be controlled with the range from 2 to 4 um by changing spinning parameters, such as the high voltage, the air pressure, the precursor solution viscosity. In this article, by the addition of alumina, the obtained fibers had continuous morphologies with certain flexible property. The adsorption behavior was investigated by varying the initial MO concentration, contact time and initial PH. It exhibited a high adsorption capacity in MO dye adsorption. Such flexible hollow CeO_2/Al_2O_3 fibers could be regarded as a favorable adsorbent for dye separation.

2. Experimental

2.1 Preparation of precursor sol

All reagents were purchased commercially and used without further purification. Magnetic stirring was employed throughout this work. 4 g $AlCl_3$ $6H_2O$ (analytical grade) was dropped into 20 g deionized water. Then 2 g aluminum powder (w（Al）＞99.5%) was added into the above solution with stirring at 80 ℃ for 6 h. Meanwhile, 0.5 g colloidal silica sol (w(SiO_2) = 25～26%) and 0.1 g polyvinyl alcohol (PVA, Mw=150000) were added. Constant stirring was required at room temperature until the formation of a uniform and stable solution (Solution A). The Solution B was prepared by adding 5 g Ce $(NO_3)_3 \cdot 6H_2O$ (analytical grade) and 2 g polyvinyl pyrrolidone (PVP, Mw=1300000) into 12 g deionized water with stirring for 4 h at room temperature. Then, Solution A was mixed with Solution B in different ratio1:2, 1:4 and 1:8 by vigorous stirring and the solution viscosity were 4.0, 2.75 and 1.6 Pa.s, respectively. The uniform mixture solution, as the shell spinning sol, was formed (Solution C). The sesame oil purchased from supermarket was used as core solution (solution D).

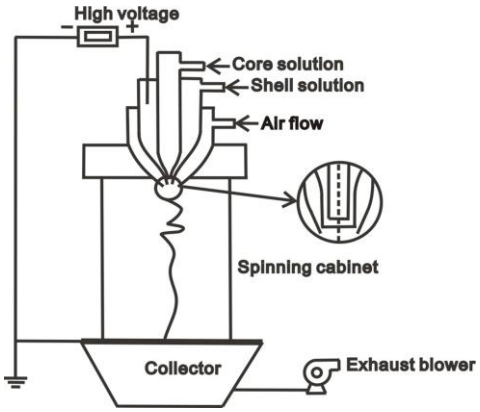

Fig.1 Schematic of self-made electrospinning apparatus

2.2 Fabrication of composite fibers

The spinning apparatus was shown in Fig.1. Solution C was injected into shell stainless needle (i.d. 1.06 mm, o.d. 1.65 mm) with 30 mL/h flow rate and Solution D was injected into core stainless needle (i.d. 0.31 mm, o.d. 0.56 mm) with 6 mL/h flow rate simultaneously. The solution flow rate can reach several times compared with conventional coaxial electrospinning [17].The distance between needle tip and collector plate was fixed at 80 cm. The solution was stretched by applying the air flow and high-voltage at a certain value to attenuate the fibers. The as-spun fibers were collected on the porous nonwoven mat after solvent evaporation. The fibers were dried at 80 ℃ for 12 h and then sintered at 600 ℃ with a heating rate of 5 ℃/min. Finally, hollow CeO_2/Al_2O_3 composite fibers were obtained.

2.3 Adsorption experiments

A series of experiments concerning the adsorption efficiency were carried out in dark condition at room temperature. The adsorption capacity of CeO_2/Al_2O_3 composite fibers was examined in terms of MO dye removal efficiency. The initial concentrations of MO solution were in the range of 10-50 mg/L. The effect of PH on adsorption was discussed by varying the PH from 2.0 to 10.0. 60 mg CeO_2/Al_2O_3 composite fibers were dispersed in 250 mL MO aqueous solution in a glass reactor. The solution was stirred in dark condition for 1 h. The concentrations of the MO solution were monitored by measuring the absorbance of solutions with a UV–vis spectrometer. The adsorption quantity of dye adsorbed onto fibers and removal

efficiency were calculated by Eqs.1-2:

$$q = \frac{(C_0 - C) \times V}{m} \quad (1)$$

$$R = \frac{(C_0 - C)}{C_0} \times 100\% \quad (2)$$

Where C_0 (mg/L) was the initial concentration of MO solution, C (mg/L) was the concentration of solution at any time, q was the adsorption quantity of dye adsorbed onto fibers, V was the volume of solution and m is the mass of CeO_2/Al_2O_3 fibers, R was the removal efficiency.

3. Results and discussion

3.1 Characterization of CeO_2/Al_2O_3 fibers

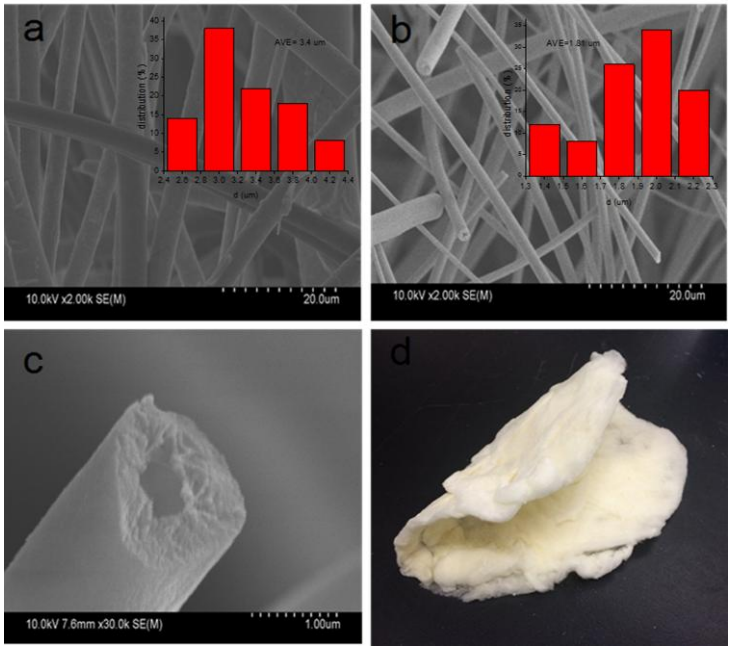

Fig.2 (a) SEM image of as-spun fibers (b) CeO_2/Al_2O_3 composite fibers sintered at 600 ℃ (c) SEM cross-sectional image(d) Digital image of CeO_2/Al_2O_3 composite fibers.

Fig.2 showed the morphologies of CeO_2/Al_2O_3 fibers. Fig.2a and b showed the SEM images of as-spun fibers and flexible hollow CeO_2/Al_2O_3 fibers, respectively. The morphology of as-spun fibers which had continuous line feature and the average diameter was 3.4 um. However, there were some cracks on the surface of fibers mainly due to the fast and imbalanced evaporation of solvents. After sintered at 600℃,

the continuous structures of fibers with smooth surface were maintained as well. The average diameter of fibers reduced to 1.81 um due to the evaporation of solvents and the decomposition of organic groups. As shown in Fig.2c, hollow structure was obviously presented. This structure was beneficial to increase the adsorption capacity of the dye molecules. Fig.2d was the digital image of CeO_2/Al_2O_3 composite fibers. By the addition of Al_2O_3, the fibers were fluffy and can be folded twice which indicated they had excellent flexibility. It is convenient for recycling after treated wastewater due to the fibers good flexibility.

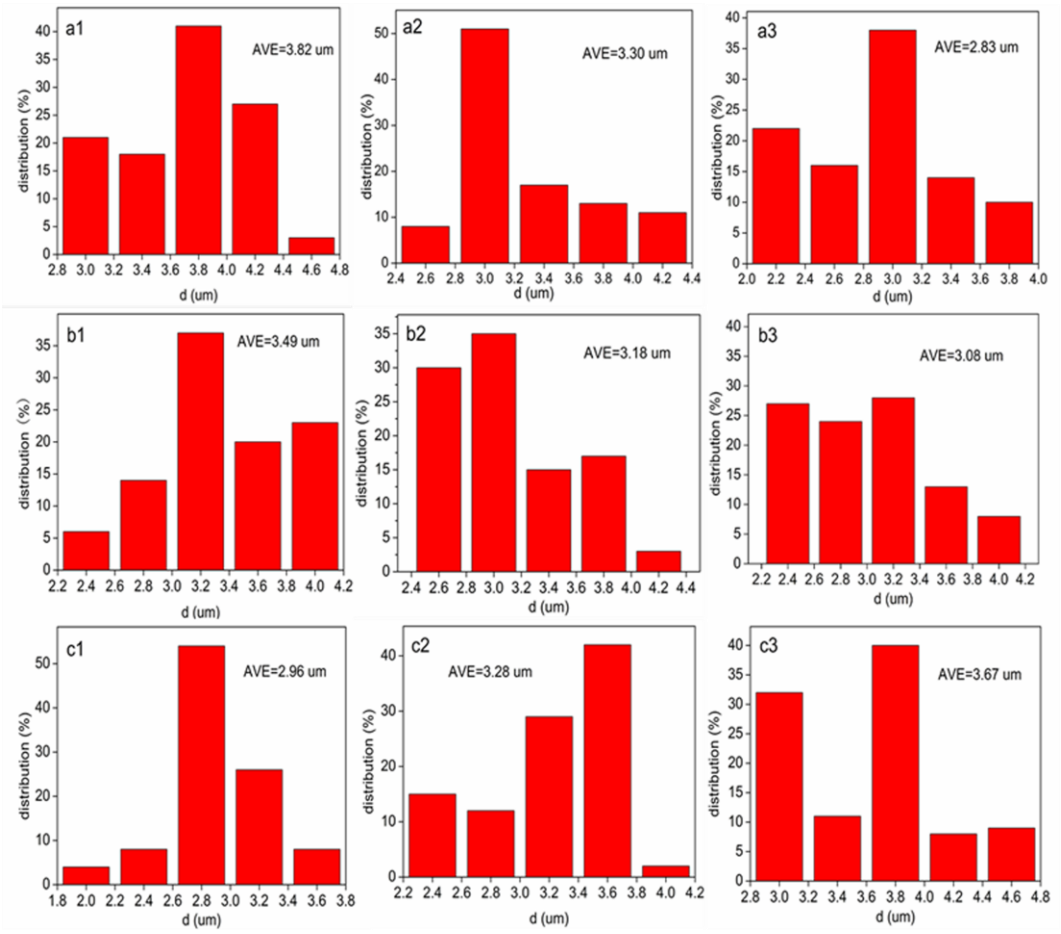

Fig.3 (a) The effects of different air pressures on as-spun fibers diameter (a1) 0.04 Mpa (a2) 0.08 Mpa (a3) 0.12 Mpa (b) The effects of different voltages on as-spun fibers diameter (b1) 30 kV (b2) 35 kV (b3) 40 kV (c) The effects of different viscosities on as-spun fiber diameter (c1) 1.6 Pa.s (c2) 2.75 Pa.s (c3) 4.0 Pa.s

The effects of spinning parameters on fibers diameter were studied through changing only a single

variable at a time. Fig.3a showed the diameter distribution of fibers prepared from different air pressure. If the air pressure was 0.04 Mpa, the average diameter of the obtained fibers was 3.82 um. When the air pressure increased to 0.08 and 0.12 Mpa, the fibers diameter reduced to 3.30 and 2.83 um, respectively. The results indicated that the fibers diameter decreased as the air flow speeded up. The solution jets were attenuated by high velocity air flow, helping to accelerate solvent evaporation. It was an important factor for the formation of fibers. A higher air pressure would form droplets during the spinning process. The optimum air pressure should be appropriate to generate fibers. To evaluate the effects of voltage on fibers diameter, three different voltages 30, 35 and 40 kV were investigated in this experiment. As shown in Fig.3b, the fibers diameter decreased from 3.49 to 3.08 um as the voltage increased. At 30 kV, the most fibers diameter distribution was 2.2 to 4.2 um with the average diameter of 3.49 um. When the voltage increased to 35, 40 kV, the fibers average diameter decreased to 3.18, 3.08 um, respectively. The tendency was in agreement with previous studies in electrospinning [25]. However, when voltage was greater than 40 kV, the solution jets became unstable and it would also cause the discharge phenomenon. The shell solution viscosity was another crucial factor that influenced the diameter of the fibers (Fig.3c). When the solution viscosity varied from 1.6 to 2.75 and 4.0 Pa.s, the fibers average diameter accordingly varied from 2.96 to 3.28 and 3.67 um. That is to say higher solution viscosity often resulted in lager fibers diameter. But the solution jets were not continuous and the needle was blocked if the viscosity exceeded 4.0 Pa.s.

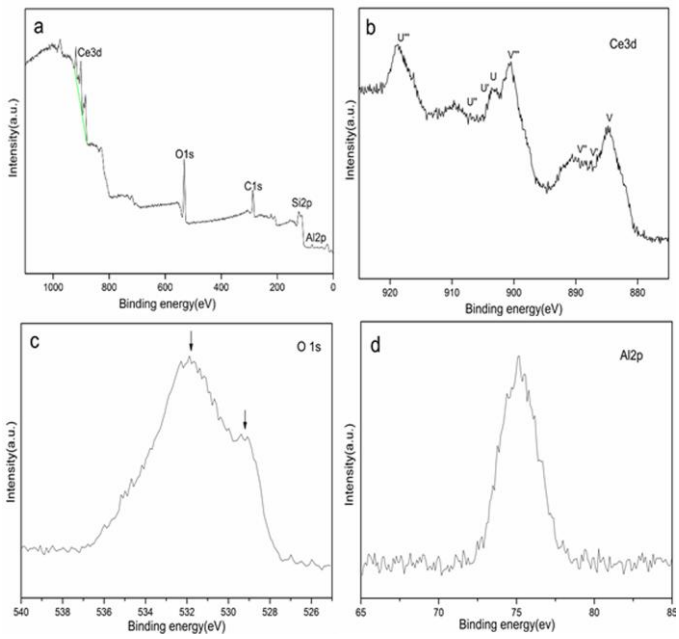

Fig.4 (a) XPS spectra of CeO_2/Al_2O_3 composite fibers (b) High resolution XPS spectra of Ce 3d (c) High resolution XPS spectra of O 1s (d) High resolution XPS spectra of Al 2p

XPS spectrum was shown in Fig.4, giving the surface composition and the constituent element valance state. The peaks of Ce 3d, O 1s, Al 2p were all presented in Fig.4a. The Ce 3d, O 1S, Al 2p high-resolution XPS spectra were shown in Fig.4b, Fig.4c and Fig.4d, respectively. The peaks labeled U, U'', U'', (V, V'', V'') refer to $3d_{3/2}(3d_{5/2})$ were corresponded to Ce^{4+} 3d final states. The peaks of Ce^{4+} located at 916.1 eV (U'', $3d_{3/2}$) and 898.2 eV (V'', $3d_{5/2}$) can be assigned to Ce ($3d^9 4f^0$) O($2p^6$) final states. The lower peaks of Ce^{4+} located at 906.9 eV (U'', $3d_{3/2}$) and 888.2 eV (V'', $3d_{5/2}$) which resulted from Ce ($3d^9 4f^1$) O ($2p^5$) final states. The additional peaks of U and V at 900.2 eV ($3d_{3/2}$) and 881.7 eV($3d_{5/2}$) were attributed to Ce ($3d^9 4f^2$) O ($2p^4$) final states from Ce^{4+}. In the case of Ce 3d of Ce^{3+}, the peaks appear at 901.7 eV (U', $3d_{3/2}$) and 883.6 eV (V', 3 $d_{5/2}$), corresponding to Ce ($3d^9 4f^1$) O ($2p^6$) final states [26]. All these peaks proved the presence of CeO_2. As shown in Fig.4c, the O 1s XPS spectra showed broad and complicated peaks because of surface oxygen species. The peaks located at 528.9 eV were corresponded to the lattice oxygen. The peaks at 531.6 eV belonged to surface hydroxyl group [27]. In Figure.4d, the

peaks located at 73.6 eV were corresponded to Al 2p spectrum, which indicated the existence of Al_2O_3.

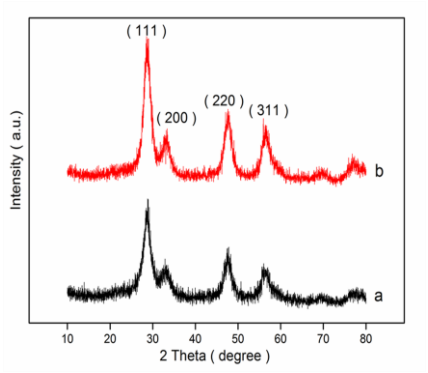

Fig.5 XRD patterns of CeO_2/Al_2O_3 composite fibers (a) before adsorption (b) after adsorption

Fig.5 gave the XRD patterns of composite fibers before adsorption and after adsorption sintered at 600 ℃, respectively. There were not any appreciable changes and no other peaks corresponding to impurities appeared. The results indicated that the fibers didn't change its chemical structures after adsorption of MO. The XRD pattern indicated the fluorite cubic phase of CeO_2. The diffraction peaks discovered at 2θ=28.6, 33.0, 47.5, 56.3 can be attributed to the (111), (200), (220), and (311) planes, respectively [28-30]. There were no district diffraction peaks corresponding to Al_2O_3, which might due to the small particle size of Al_2O_3 in the composite fibers [31].

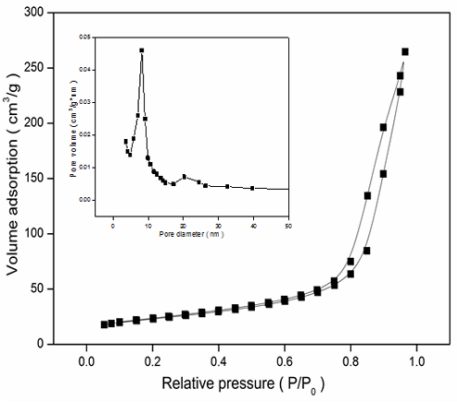

Fig.6 Nitrogen adsorption-desorption isotherm and pore size distribution curve of CeO_2/Al_2O_3 composite fibers

Surface area and pore size were vital properties in the application of adsorption. Higher surface area provided more active sites which was beneficial for the adsorption of dye molecules. To measure the surface area and porosity of hollow CeO_2/Al_2O_3 fibers, N_2 adsorption-desorption

isotherm was investigated (Fig.6). The surface area of fibers was 121m^2/g. The BET results revealed the fibers had higher surface area. The pore size distribution was calculated from the adsorption isotherms using Bareett-loyner-Halenda (BJH) analysis and described in the picture of Fig.6. It can be seen that the pore size was ranged from 5 to 40 nm and the average pore diameter was 14.35 nm.

3.2 Adsorption experiments

3.2.1 The effects of initial concentrations of MO and adsorption isotherms

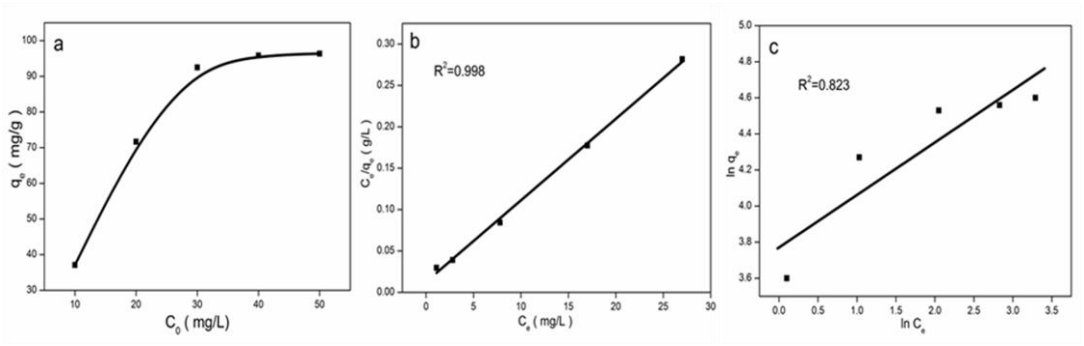

Fig.7 (a) Effects of initial concentrations on equilibrium adsorption capacity (b) Plots based on Langmuir isotherm model (c) Freundlich isotherm model

The effects of the initial concentrations over the range (10-50 mg/L) on adsorption were investigated in Fig.7, where 60 mg of CeO_2/Al_2O_3 fibers were added to 250 ml of MO solution at PH 4. The results showed that the equilibrium adsorption capacity increased gradually with the increase of initial MO concentrations until it reached to a certain level. At lower concentrations, the increase of the adsorption capacity can be attributed to the increase in the driving force of concentration gradient. Adsorption capacity did not change when the initial concentration reached to 40 mg/L. Because a large number of active sites were fully occupied, the adsorption quantity reached saturation.

The Langmuir and Freundlich were two widely used models to describe the interactions between adsorbates and sorbents and predicted the mechanism of the adsorption [32]. The Langmuir and

Freundlich equations can be expressed by Eqs.3-4, respectively.

$$\frac{C_e}{q_e} = \frac{C_e}{q_m} + \frac{1}{K_L \times q_m} \quad (3)$$

$$\ln q_e = \ln K_F + \frac{1}{n \times \ln C_e} \quad (4)$$

Where q_e (mg/g) was the equilibrium amount of adsorbed MO and C_e(mg/L) was equilibrium concentration of MO, q_m(mg/g) was the adsorption capacity which were evaluated from the slope. The constant K (K_L, K_F) and n indicated the extent of adsorption and the adsorption effectiveness, respectively. The Langmuir model represented that the adsorption was limited to homogeneous coverage. The Freundlich model related the adsorption surface on fibers was heterogeneous, that revealed multilayer adsorption [32]. Based on the correlation coefficients (R^2) and the fitted curves (Fig.7b and c), the results revealed that Langmuir isotherm (R^2=0.998) fitted the data better than Freundlich isotherm (R^2=0.823). The adsorption capacity (q_m) calculated by Langmuir was 104 mg/g. The experimental data matched well with the Langmuir isotherm, which indicated the single layer adsorption.

3.2.2 The effects of time and adsorption kinetics

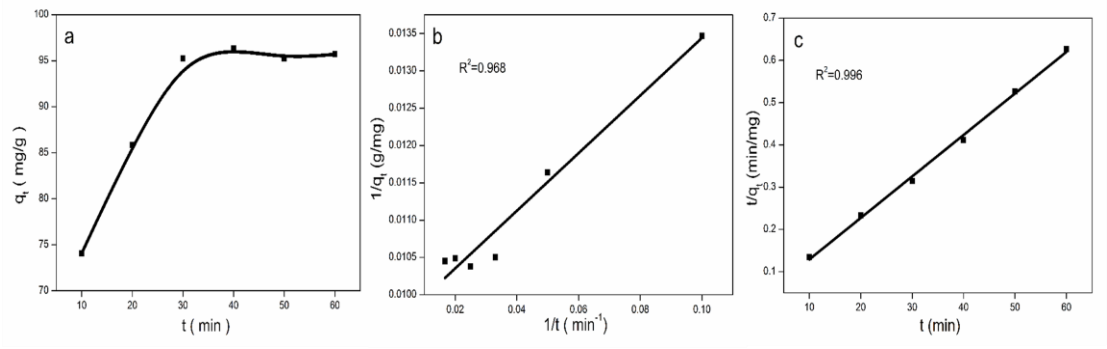

Fig.8 (a) Effect of time on adsorption of MO onto the hollow CeO_2/Al_2O_3 fibers (b) Plots based on pseudo-first-order kinetic model (c) pseudo-second-order kinetic model

The effects of contact time on the adsorption capacity were discussed and shown in Fig.8a, where

60 mg of CeO_2/Al_2O_3 fibers were added to 250 ml of MO solution (30 mg/L) at PH 4. The adsorption quantity of MO was increased rapidly at the beginning, due to the large number active sites on fibers surface. It gradually increased with time increasing until it reached adsorption equilibrium (q_e=95.7 mg/g) after 60 min. Zou et.al fabricated $CuFe_2O_4$@CeO_2 nanofibers to adsord MO solution, the reported adsorption capacity was 100.0 mg/g and equilibrium time was 700 min. Compared with this results, the equilibrium adsorption capacity was the same as Zou, but the equilibrium time (60 min) was obviously shorter than his report [33]. At equilibrium, the number of active sites on fibers surface decreased and were difficult to be occupied by MO molecules.

In order to better understand the mechanism and behavior of adsorption, the adsorption kinetics was studied because it controlled the equilibrium and efficiency of adsorption process. The pseudo-first-order and pseudo-second-order models were expressed as follows:

$$\frac{1}{q_t} = \frac{1}{q_e} + \frac{K_1}{q_e \times t} \qquad (5)$$

$$\frac{t}{q_t} = \frac{1}{K_2 \times q_e^{\ 2}} + \frac{t}{q_e} \qquad (6)$$

Where k (k_1, k_2) was the adsorption rate constant, q_e and q_t were the adsorption amounts of MO at equilibrium at any time t (min). The linear regression was presented in Fig.8b and c. The correlation coefficients (R^2=0.996) of pseudo-second-order was higher than pseudo-first-order (R^2=0.968), indicating that the pseudo-second-order model fitted better the adsorption data. By the pseudo-second-order model, it can be concluded that the chemical adsorption would be the rate-determining step controlling the adsorption process.

3.2.3 The effects of PH and the regeneration of adsorbent fibers

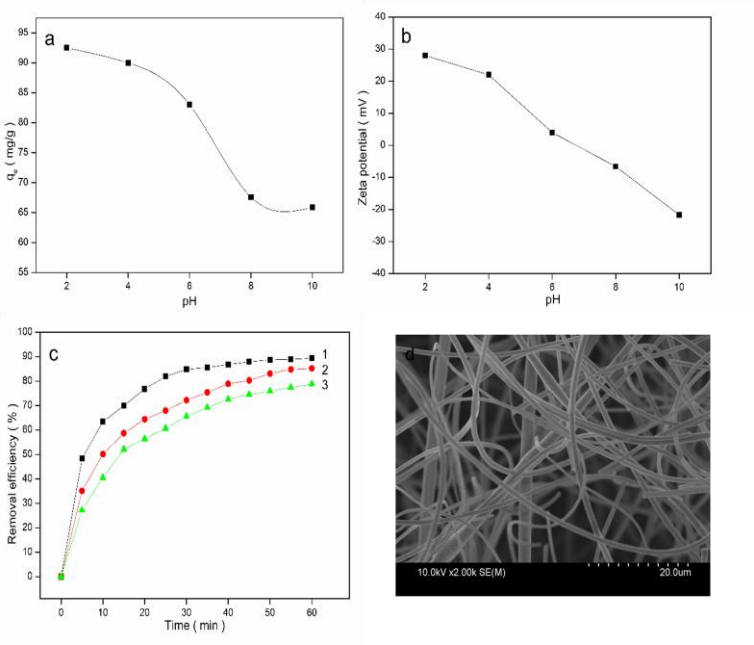

Fig.9 (a) Effects of PH on equilibrium adsorption capacity (b) Zeta potential of CeO_2/Al_2O_3 fibers at different PH (c) Reusability of fibers for MO adsorption (d) SEM image of fibers after absorbed MO dye

It was known that the PH of the dye solution was an important controlling parameter in the adsorption process, because it affected the properties of both the adsorbent fibers and the dye molecules. Fig.9a showed the influence of PH values on MO adsorption with in the range of 2-10. The experiments were performed with the MO concentration of 30 mg/L and 60 mg CeO_2/Al_2O_3 fibers in 250 ml solution at room temperature. The results indicated that the adsorption quantity decreased with the PH values increasing from 2 to 10. Moreover the adsorption quantity became a constant with the PH increasing from 8 to 10. The graph of Zeta potential of CeO_2/Al_2O_3 fibers against the PH was measured in Fig.9b. At lower PH, the surface of CeO_2/Al_2O_3 fibers had a net positive charge, which was conductive to adsorb the negative MO onto the vacant active sites. As PH increased, there was a competition of OH^- with negative MO. The active adsorption sites were closely associated with OH^- and fewer sites were available for MO molecules.

With rising prices of wastewater treatment processes, the product re-usability had increased

significantly. In this work, the used fibers were washed with deionized water three times to remove the loosely bound MO molecules and dried in 80℃ for 12 h. The experiments were performed at same conditions: initial dye concentration 30 mg/L, adsorbent fibers 60 mg, solution volume 250 mL, PH 4. From Fig.9c, the percentage removal maintained efficiency and slightly decreased. The results indicated that the fibers were stable for the 3 reused runs. Considering the above results, such strong adsorption capacity was probably due to the fibers hollow structure with higher surface area. Fig.9d showed the SEM image of used fibers, we can clearly see that the fibers still remained continuous morphologies. So when the test finished, the composite fibers were easily separated by simple filtration.

3.2.4 Adsorption mechanism

It is worth noting that the adsorption mechanism was dependent on the properties of dye molecules, adsorbent fibers and their interactions [34]. Electrostatic attraction, hydrogen bonds, van der waals forces, chemical bonding interactions might act simultaneously or individually, which played important roles in the adsorption process [35]. In aqueous solution, the surface of the fibers tended to form a positive net charge and the MO dyes would be hydrolyzed into anionic ions. According to the effects of PH, it demonstrated the involvement of electrostatic attraction, hydrogen bonds and van der waals force in the adsorption process. The adsorption isotherm and kinetics behavior suggested the adsorption was a monolayer adsorption and chemical bonding was the main driving force.

4. Conclusions

In conclusion, the flexible hollow CeO_2/Al_2O_3 composite fibers were successfully prepared by coaxial electro-blowing spinning technique. The composite fibers had certain flexible property after calcination. The composite fibers achieved desirable performance in MO dye adsorption. All of these characteristics

indicated that these composite fibers have promising applications in the treatment of dye wastewater and environmental purification.

Acknowledgments

The authors would like to thank the National Natural Science Foundation of China (51102178) for financial support in this article.

References

[1] Hameed U, Tahir H, Sultan M. Lap Lambert Academic Publishing, 2013.

[2] Behnajady M A, Bimeghdar S. Chemical Engineering Journal, 2014, 239(1):105–113.

[3] Chen R, Yu J, Xiao W. J.mater.chem.a, 2013, 1(38):11682-11690.

[4] Fan J, Zhao L, Yu J, et al. Nanoscale, 2012, 4(20):6597-6603.

[5] Beek W J E, Wienk M M, Janssen R A J. Advanced Functional Materials, 2006, 16(8): 1112-1116.

[6] Zhang J, Wang S, Wang Y, et al. Sensors and Actuators B: Chemical, 2009, 139(2): 411-417.

[7] Lu Z, Mao C, Meng M, et al. Journal of colloid and interface science, 2014, 435: 8-14.

[8] Li C, Zhang X, Dong W, et al. Materials Letters, 2012, 80: 145-147.

[9] Valášková M, Kočí K, Kupková J. Microporous and Mesoporous Materials, 2015.

[10] Eltayeb A, Vijayaraghavan R K, McCoy A, et al. Journal of Power Sources, 2015, 279: 94-99.

[11] Pontelli G C, Reolon R P, Alves A K, et al. Applied Catalysis A: General, 2011, 405(1): 79-83.

[12] Qian J, Chen F, Wang F, et al. Materials Research Bulletin, 2012, 47(8): 1845-1848.

[13] Qi zheng C, Xiang ting D, Jin xian W, et al. Journal of Rare Earths, 2008, 26(5): 664-669.

[14] L ü Q, Dong X, Zhu Z, et al. Ceramics International, 2014, 40(10): 15545-15550.

[15] Lang Y, Wang C A. Ceramics International, 2014, 40(7):10329–10335.

[16] Shen J, Li Z, Wu Y, et al. Chemical Engineering Journal, 2015, 264: 48-55.

[17] Teng M, Qiao J, Li F, et al. Carbon, 2012, 50(8):2877–2886.

[18] Schneiderman S, Zhang L, Hao F, et al. Journal of Chromatography A, 2011, 1218(50):8989-8995.

[19] Zhang Y X, Yu X Y, Jin Z, et al. J.mater.chem, 2011, 21(21):16550-16557.

[20] Zhang J, Choi S W, Kim S S. Journal of Solid State Chemistry, 2011, 184(11):3008–3013.

[21] Chang W, Xu F, Mu X, et al. Materials Research Bulletin, 2013, 48:2661–2668.

[22] Khalaf, A. Stellenbosch University of Stellenbosch (2009).

[23] Zhou F L, Hubbard P L, Eichhorn S J, et al. Acs Appl Mater Interfaces, 2012, 4(11):6311-6316.

[24] Cheng B, Tao X, Shi L, et al. Ceramics International, 2014, 40:15013–15018.

[25] Zhang S, Shim W S, Kim J. Materials & Design, 2009, 30(9):3659–3666.

[26] ZHANG J, Bing W, Hao C U I, et al. Journal of Rare Earths, 2014, 32(12): 1120-1125.

[27] Liao X, Zhang Y, Hill M, et al. Applied Catalysis A: General, 2014, 488: 256-264.

[28] Jiang B, Zhang S, Guo X, et al. Applied Surface Science, 2009, 255(11): 5975-5978.

[29] Wu C. Materials Letters, 2015, 139: 382-384.

[30] Qian J, Chen Z, Liu C, et al. Materials Science in Semiconductor Processing, 2014, 25: 27-33.

[31] Tang H, Sun H, Chen D, et al. Materials Letters, 2012, 77: 7-9.

[32] Mahapatra A, Mishra B G, Hota G. Journal of Hazardous Materials, 2013.

[33] Zou L, Wang Q, Shen X, et al. Applied Surface Science, 2015, 332:674–681.

[34] Zhang F, Zhao Z, Tan R, et al. Journal of Colloid\s&\sinterface Science, 2012, 386(22):277–284.

[35] Li J, Ng D H L, Song P, et al. Journal of Industrial & Engineering Chemistry, 2014.